



## Re-dissolution and re-precipitation behavior of nano-precipitated phase in Al–Cu–Mg alloy subjected to rapid cold stamping

Cai-he FAN<sup>1</sup>, Ling OU<sup>1</sup>, Ze-yi HU<sup>1</sup>, Jian-jun YANG<sup>1</sup>, Xi-hong CHEN<sup>2</sup>

1. College of Metallurgy and Material Engineering, Hunan University of Technology, Zhuzhou 412007, China;

2. CRRC Zhuzhou Electric Locomotive Co., Ltd., Zhuzhou 412007, China

Received 11 April 2019; accepted 17 September 2019

**Abstract:** High-resolution transmission electron microscopy (TEM), X-ray diffractometry (XRD), energy dispersive spectroscopy (EDS) and hardness test were used to study the re-dissolution and re-precipitation behavior of nano-precipitates of the spray-formed fine-grained Al–Cu–Mg alloy during rapid cold stamping deformation. Results show that the extruded Al–Cu–Mg alloy undergoes obvious re-dissolution and re-precipitation during the rapid cold-stamping deformation process. The plastic  $\theta'$  phase has a slower re-dissolution rate than the brittle  $S'$  phase. The long strip-shaped  $S'$  phases and the acicular  $\theta'$  phases in Al–Cu–Mg alloy after three passes of cold stamping basically re-dissolved to form a supersaturated solid solution. A large number of fine granular balance  $\theta$  phases precipitate after four passes of rapid cold-stamping deformation. Rapid cold stamping deformation causes the  $S'$  phase and  $\theta'$  phase to break and promote the nano-precipitate phases to re-dissolve. The high distortion free energy of the matrix promotes the precipitation of the equilibrium  $\theta$  phase, and the hardness of the alloy obviously increases from HB 55 to HB 125 after the rapid cold stamping process.

**Key words:** Al–Cu–Mg alloy; rapid cold stamping; nano-precipitate; re-dissolution; re-precipitation

### 1 Introduction

Al–Cu–Mg alloy has been widely used in aerospace and military fields due to its high strength, formability and heat resistance [1,2]. As an important means for improving the microstructure of aluminum alloys and obtaining micron and nano-scale fine-grained materials, strong plastic deformation (SPD) technology has been widely explored [3–8]. Second-phase dissolution caused the matrix to become a supersaturated solid solution during the SPD of Al–Cu alloy [9–17]. With a continuous strong deformation or re-aging of this alloy, new second phases precipitate again as fine particles, which significantly improve the mechanical properties of the alloy. NOURBAKSH and NUTTING [9] found that the flaky  $\theta'$  phase in Al–4%Cu alloy is severely bent and broken after a considerable reduction of the cold rolling. SENKOV et al [10] firstly discovered the re-dissolution of  $Al_3Fe_4$  phase in the Al–Fe alloy during strong plastic deformation at low temperatures. MURAYAMA et al [11] studied the equal-diameter

extrusion deformation of an Al–Cu binary alloy, and found that a needle-like  $\theta'$  transition phase gradually decomposes into short-chain particles and dissolves back into the matrix during several passes of equal-diameter extrusion. ZHANG et al [12,13] studied the effects of multi-directional compression deformation on the precipitates of Al–Cu alloy. The re-dissolution of the precipitated phase induced by strong plastic deformation forms a supersaturated solid solution. The re-precipitation sequence of the phase, the heating temperature, and the deformation degree are related to grain size after deformation. XU et al [14,15] investigated the re-dissolution and re-precipitation behavior of  $\theta''$  phase,  $\theta'$  phase, and  $\theta$  phase of Al–Cu alloy via equal-diameter extrusion deformation at a normal temperature, and found that  $\theta''$  phase has the fastest dissolution rate. The  $\theta$  phase has the slowest rate of dissolution, and the  $\theta$  phase will precipitate if strong deformation occurs. STYLES et al [16] explored the relationship between the resolution sequence of the supersaturated solid solution and the equilibrium  $S$  phase in the Al–Cu–Mg alloy. The formation time of  $S$  phase at

high temperature is shorter than that at low temperatures. The re-dissolution of the second phase of Al–Cu alloy in strong deformation is an important microscopic phenomenon, which is of great significance for further exploring the strengthening mechanism of the alloy and the development of a new heat treatment process.

In order to proceed further research and exploration on this phenomenon, based on rapid solidification fine-grained Al–Cu–Mg alloy billet by spray forming, the effect of rapid cold-stamping on the re-dissolution and re-precipitation behavior of the nano-precipitated phase in Al–Cu–Mg alloy was studied, and the correlation between the hardness change of the alloy and the re-dissolution and re-precipitation of the phase was analyzed.

## 2 Experimental

The rapidly solidified fine-grained Al–Cu–Mg alloy cylindrical ingot was prepared on a self-developed SD380 large-scale injection molding apparatus. The chemical composition of the alloy is shown in Table 1. The cylindrical ingot was extruded into a  $d30$  mm round bar on a 1250 T extruder at a temperature of  $450$  °C and an extrusion ratio of 15:1. The round bar was cut into a small cylinder of  $d30$  mm  $\times$  20 mm and rapidly cold stamped for four passes at  $25$  °C. The schematic diagrams of rapid cold stamping are illustrated in Fig. 1. The parameters of the rapid cold stamping are shown in Table 2.

**Table 1** Chemical composition of alloy (wt.%)

Cu	Mg	Mn	Si	Fe	Al
4.0	1.7	0.40	<0.03	<0.03	Bal.

The samples were obtained on the wall of the rapid cold forming cylinder for microstructure observation and hardness testing. The morphology, size and distribution of the nano-precipitated phase of the sample were analyzed through a JEM–F200 transmission electron microscope (TEM). The transmission sample was mechanically pre-thinned to approximately  $80$   $\mu$ m, electrolyzed, and double-sprayed. The electrolytes were nitric acid and methanol (volume ratio of 1:3), at a temperature lower than  $-25$  °C. The electron microscopy parameters of the high-angle annular dark field scanning transmission electron microscope (HAADF–STEM) were as follows: acceleration voltage of 200 keV, electron beam half convergence angle of 10 mrad, high-angle annular probe for collecting the inner half angle of 36 mrad, and a beam spot diameter of 0.20 nm. The phase identification was analyzed by a D/max 2500 18 kW target X-ray diffractometer. The Brinell hardness

of the sample was tested by using a HBRV–187.5 electric Blowell hardness tester. The hardness values are the average values of 6 points in each sample, and the measurement position is the middle part of the outer surface of the cylinder wall.

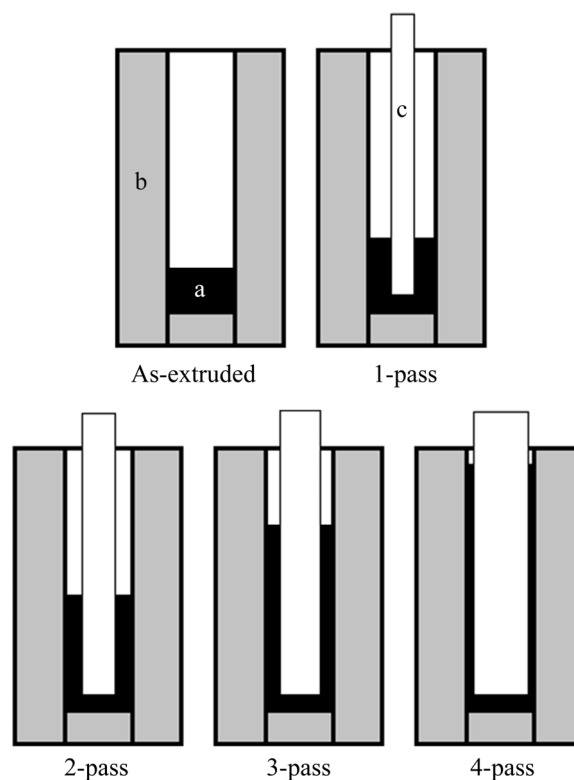


**Fig. 1** Sketch maps of rapid cold stamping process: a–Sample; b–Drawing die; c–Punch

**Table 2** Technological parameters of rapid cold stamping

Punch pass	Diameter/mm	Velocity/(mm·s <sup>-1</sup> )
1	10	30
2	14	25
3	20	20
4	27	15

## 3 Results

### 3.1 Hardness curve

The hardness curve of Al–Cu–Mg alloy after different passes of cold stamping deformation is shown in Fig. 2. The hardness value of the extruded alloy during the rapid cold stamping deformation significantly increases from HB 55 to HB 125, which increases by 127%. The two stages with the fastest increase in hardness value are the first pass and the fourth pass. The hardness values in the second and third passes increase slightly, and the growth rate is small, especially the hardness of the alloy also shows a slight decrease in the third pass during the stamping process.

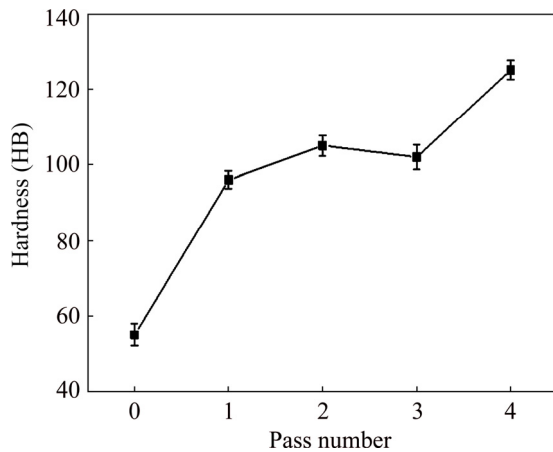


Fig. 2 Hardness as function of various passes of rapid cold stamping process

### 3.2 XRD pattern

The XRD patterns of Al–Cu–Mg alloy after different passes of cold stamping are shown in Fig. 3. As the number of passes increases, the peak value of the precipitated phase in the alloy matrix firstly decreases and then increases. The main precipitates of the extruded Al–Cu–Mg alloy are  $\text{Al}_2\text{CuMg}$  phase and the  $\text{Al}_2\text{Cu}$  phase, and the type of the phase and the diffraction peak intensity after one pass of rapid cold stamping deformation have no obvious change compared to the extruded state of the alloy. The diffraction peak intensities of  $\text{Al}_2\text{CuMg}$  phase and  $\text{Al}_2\text{Cu}$  phase obviously are weakened after two passes. After three passes of rapid cold stamping deformation, the  $\text{Al}_2\text{Cu}$  phase in the alloy disappears, and the peak strength of  $\text{Al}_2\text{CuMg}$  phase has been very small. The  $\text{Al}_2\text{CuMg}$  phase and the  $\text{Al}_2\text{Cu}$  phase re-precipitate in the alloy matrix after four passes of rapid cold-stamping deformation.

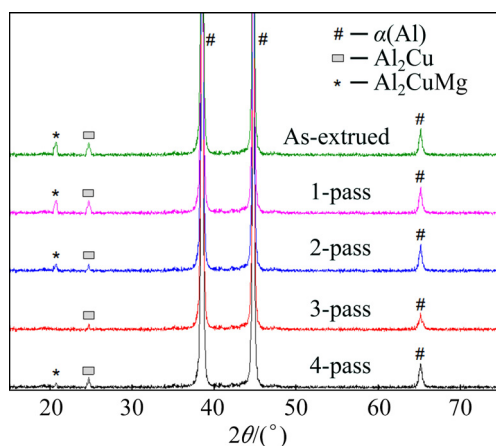


Fig. 3 XRD patterns of Al–Cu–Mg alloy samples undergoing various passes of rapid cold stamping process

### 3.3 TEM and EDS observation

The HAADF–STEM and EDS diagrams of the

Al–Cu–Mg alloy as-extruded, after three and four passes of rapid cold stamping are shown in Figs. 4, 5 and 6 respectively. It can be seen from Fig. 4 that after the hot-extrusion, the nano-precipitates in the Al–Cu–Mg alloy matrix are mainly the elongated  $S'$  phase ( $\text{Al}_2\text{CuMg}$  phase) and the needle-like  $\theta'$  phase ( $\text{Al}_2\text{Cu}$  phase). And a small number of fine granular  $S$  and  $\theta$  phases can also be observed. From Fig. 5, the extruded Al–Cu–Mg alloy undergoes significant re-dissolution of precipitate after three passes of rapid cold stamping deformation, and the long strip-shaped  $S'$  phase and the needle-like  $\theta'$  phase disappear substantially. A small number of fine granular particles are observed, as indicated by the arrows in Fig. 5. As shown in Fig. 6, the re-precipitation behavior occurs in the extruded Al–Cu–Mg alloy after 4 passes of rapid cold stamping deformation. The re-precipitated phase in the alloy matrix is mainly the granular equilibrium phase  $\theta$  phase, and the equilibrium  $S$  phase is rarely observed. The results of Figs. 4–6 are in consistence with those of Fig. 3.

## 4 Discussion

### 4.1 Re-dissolution mechanism of nano-precipitated phase during rapid cold stamping

In this experiment, rapid cold stamping deformation has three major characteristics: low deformation temperature (25 °C), large strain, and high strain rate. Previous studies [14,15] showed that Al–Cu alloy undergoes strong plastic deformation at low temperature; the larger the strain and strain rate are, the faster the dissolution rate of the precipitated phase in the alloy will be. VASILS et al [17] believed that two kinds of changes occur when precipitates completely dissolve into the matrix: one is lattice transformation in which the lattice of the precipitated phase changes into the matrix lattice; the other is the diffusion of the re-dissolved solute atom in the matrix, thereby making the supersaturated solid solution more uniform. Figures 4–6 show that the  $S'$  and  $\theta'$  phases in the as-extruded alloy basically re-dissolve into the aluminum matrix after three passes of rapid cold stamping deformation and saturated solid solution forms. Obviously, the rapid cold stamping deformation temperature of the alloy in this test is low, while the solute atoms are uniformly dispersed into the matrix by diffusion to achieve the re-dissolution of the precipitate phase, so the speed must be very slow.

According to Refs. [18,19], the  $\text{Al}_2\text{Cu}$  phase is a plastic phase, while the  $\text{Al}_2\text{CuMg}$  phase is a typical brittle phase. Under the condition of rapid cold stamping deformation, the long strip-shaped  $S'$  phase in the extruded Al–Cu–Mg alloy is obviously broken and separated (Figs. 7(a) and (b)), and the acicular  $\theta'$  phase is bent, broken and separated (Figs. 7(c) and (d)). It can be

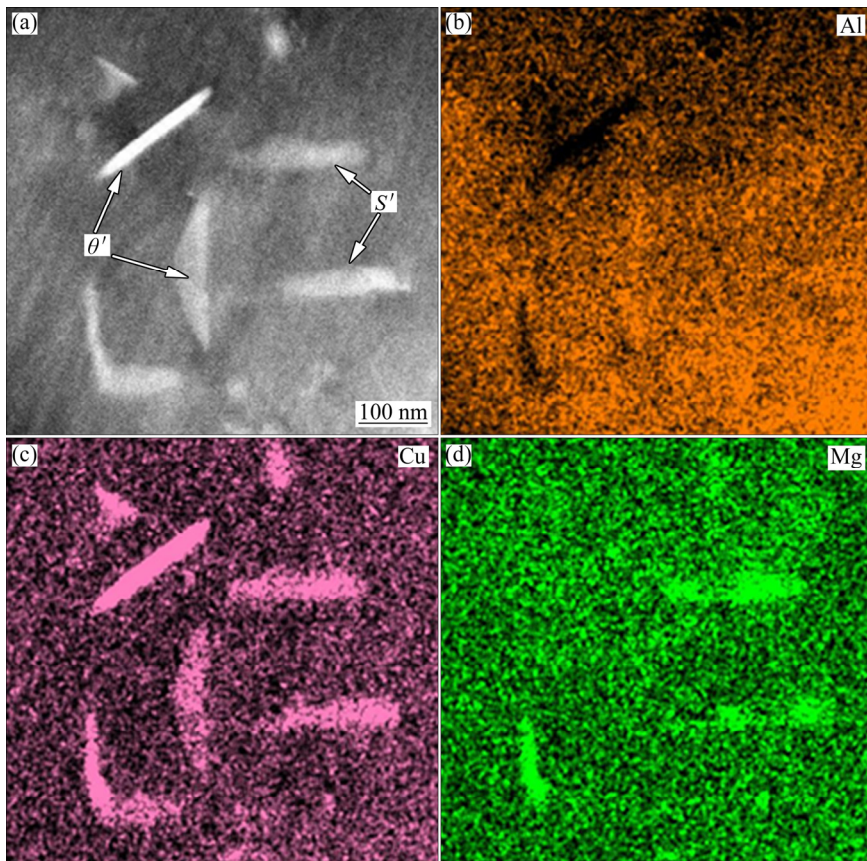


Fig. 4 HAADF-STEM image (a) and EDS maps (b-d) of precipitated phase in as-extruded Al-Cu-Mg alloy

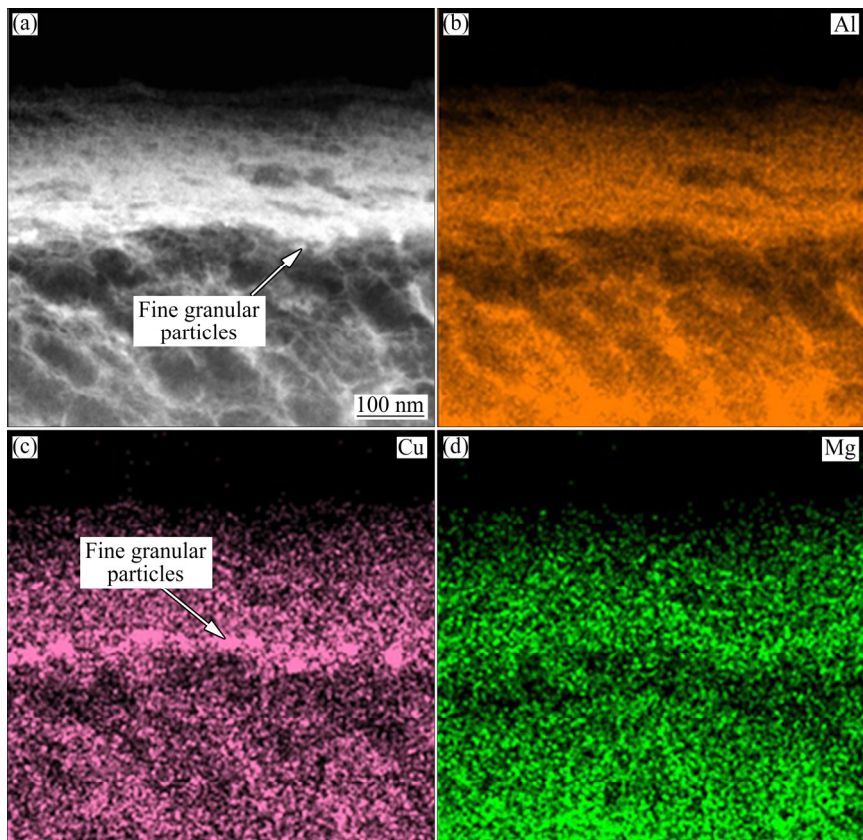
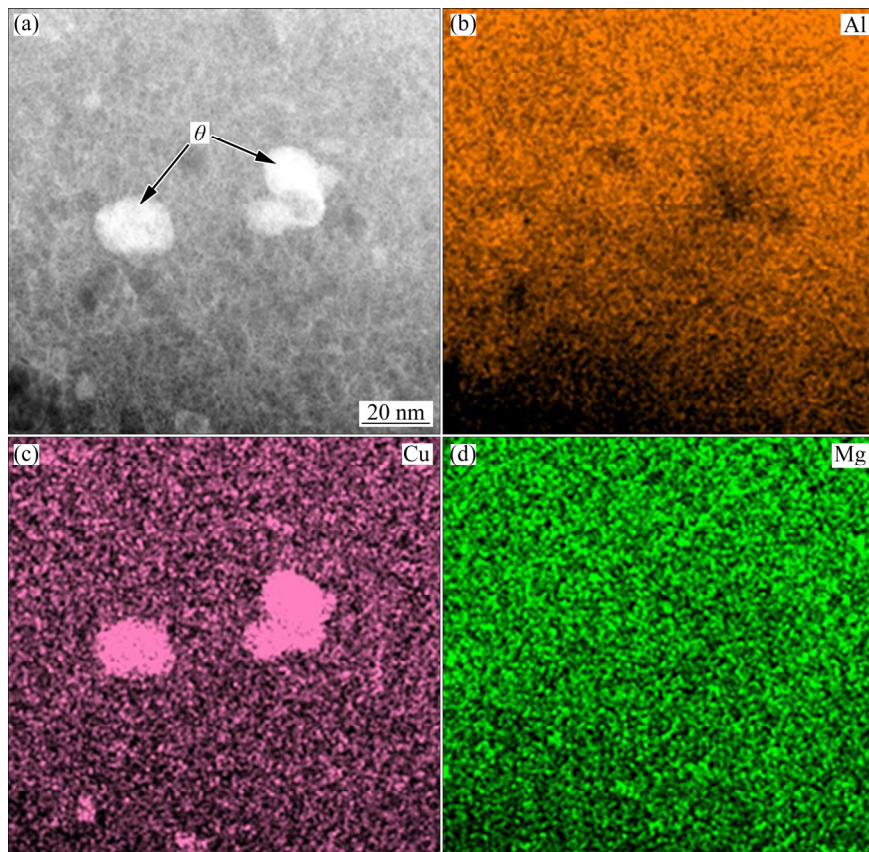
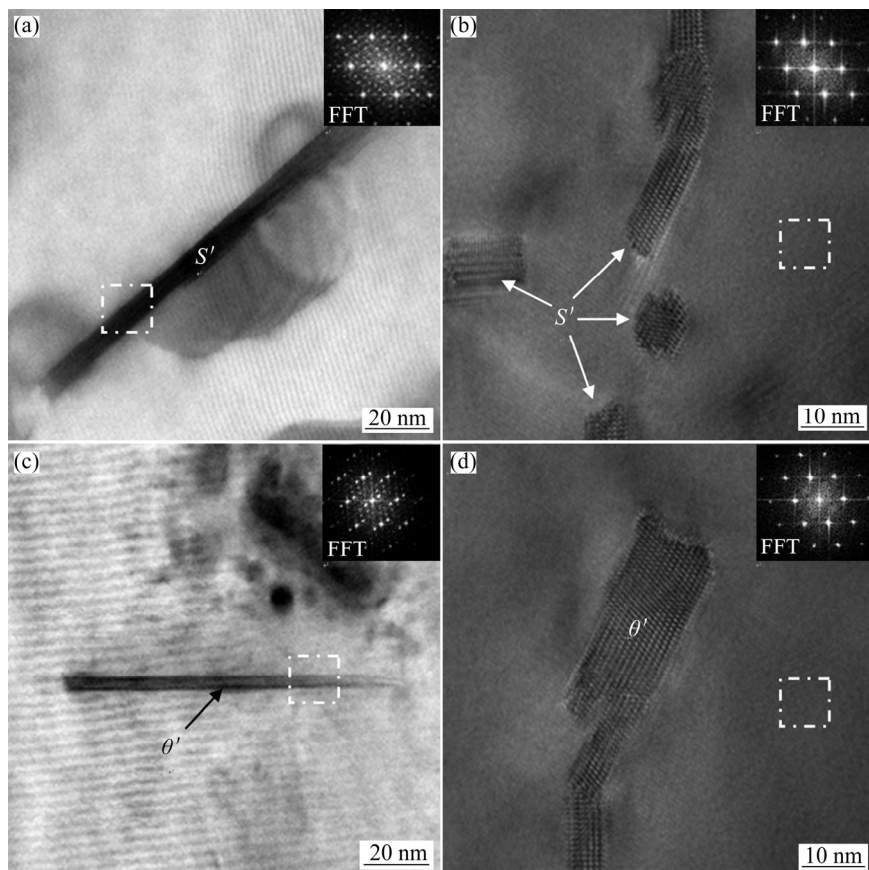


Fig. 5 HAADF-STEM image (a) and EDS maps (b-d) of precipitated phase in Al-Cu-Mg alloy undergoing 3-pass



**Fig. 6** HAADF-STEM image (a) and EDS maps (b-d) of precipitated phase in Al-Cu-Mg alloy undergoing 4-pass



**Fig. 7** TEM and FFT images of  $S'$  and  $\theta'$  precipitated phase undergoing extrusion (a, c) and 2-pass of rapid cold stamping deformation (b, d)

seen from Fig. 7 that the curvature radius of the fractured and curved precipitated phase increases significantly, the contact surface between the precipitated phase and the matrix increases remarkably, and the interface distortion can be significantly improved. It results in the free energy of the precipitated phase being higher than that of the matrix. The energy balance between the pre-precipitated phase and the matrix is broken, thus creating conditions for the solute atoms to dissolve back into the matrix. The binding energy  $E_{\text{coh}}$  and formation enthalpy  $\Delta H$  [18,19] between the  $\text{Al}_2\text{Cu}$  phase and the  $\text{Al}_2\text{CuMg}$  phase are calculated by the first principle:

$$E_{\text{coh}} = E_{\text{total}}^{\text{AB}} - [x_{\text{A}} E_{\text{atom}}^{\text{A}} + (1 - x_{\text{A}}) E_{\text{atom}}^{\text{B}}] \quad (1)$$

$$\Delta H = E_{\text{total}}^{\text{AB}} - [x_{\text{A}} E_{\text{solid}}^{\text{A}} + (1 - x_{\text{A}}) E_{\text{solid}}^{\text{B}}] \quad (2)$$

where  $E_{\text{total}}^{\text{AB}}$  is the average energy per atom of each intermetallic compound;  $E_{\text{atom}}^{\text{A}}$  and  $E_{\text{atom}}^{\text{B}}$  are the energies of free atoms A and B, respectively; and  $E_{\text{solid}}^{\text{A}}$  and  $E_{\text{solid}}^{\text{B}}$  are the average energies per atom in stable elemental A and B, respectively;  $x_{\text{A}}$  represents the mole fraction of atom A in the compound. The calculation in Ref. [20] shows that the absolute value of binding energy for  $\text{Al}_2\text{Cu}$  phase is larger than that of  $\text{Al}_2\text{CuMg}$  phase, which indicates that the  $\text{Al}_2\text{Cu}$  phase is more stable and needs more energy to decompose or re-dissolve it. This is consistent with the results of Fig. 7. After 2 passes of rapid cold stamping deformation, the  $S'$  phase is easily broken, and it is more likely to re-dissolve. The re-dissolution rate of the  $\theta'$  phase is significantly slower than that of the  $S'$  phase.

In accordance with solid phase transition theory [20], the critical size of the nucleus  $r_c$  is expressed as follows:

$$r_c = f\left(\frac{\sigma}{\Delta G} - U\right) \quad (3)$$

where  $\sigma$  is the surface free enthalpy,  $\Delta G$  is the difference in volume free enthalpy between the parent phase and the precipitated phase, and  $U$  is the strain energy produced by the two phases.

With the fragmentation of the precipitated phase,  $\sigma$ ,  $\Delta G$  and  $U$  change significantly, resulting in an increase in the critical size  $r_c$  of the precipitated phase, and the amount of re-dissolution and the re-dissolving rate of the precipitated phase increase.

In order to further analyze the re-dissolving process of the nano-precipitated phase in the rapid cold stamping  $\text{Al-Cu-Mg}$  alloy, the HAADF-STEM image of the  $S'$  phase after crushing was observed, as shown in Fig. 8. The “resolving step” on the particles after breaking can be clearly observed, and the arrows in the figure show the direction of resolving. The more the “resolving steps” are, the larger the contact surface of the broken particles with the substrate is. According to the classical

thermodynamic view [20], at any temperature, there is a certain equilibrium vacancy concentration in the crystal, and the vacancies always move positions continuously. The existence and movement of vacancies create conditions for atomic diffusion. In the rapid cold deformation process of the experimental alloy, the dislocation density increases significantly. A large number of vacancies are produced in the matrix during the delivery and movement of the dislocation, and every pass of a newly rapid cold stamping deformation will produce a large number of vacancies. At the same time, the coarser precipitated phase is continuously broken during the strong deformation process, and the interface between the precipitated phase and the matrix increases, accompanied by a large number of vacancies. Literature studies [13,21] have shown that the number of vacancies in the process of strong deformation increases sharply, the diffusion rate of solute atoms can increase by five orders of magnitude, and the volume diffusion can be increased by eight orders of magnitude. So, the “resolving step” on the broken particles further accelerates the re-dissolution of the precipitated phase.

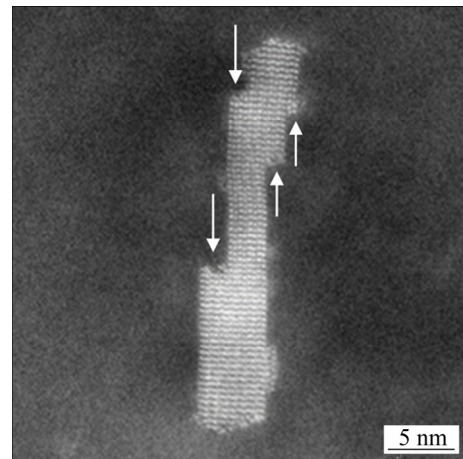


Fig. 8 HAADF-STEM image of precipitated phase in  $\text{Al-Cu-Mg}$  alloy sample

#### 4.2 Re-precipitation mechanism of nano-precipitated phase during rapid cold stamping

The experimental results show that the main precipitated  $S'$  phase and  $\theta'$  phase in the extruded  $\text{Al-Cu-Mg}$  alloy are completely re-dissolved after three passes of rapid cold stamping deformation. After the fourth pass of cold stamping deformation, a significant re-precipitation occurs, and the precipitated phase is no longer dominated by the transition phase, but dominated by the equilibrium  $\theta$  phase. During the strong deformation process, the coarse  $S'$  and  $\theta'$  fractured particles cause the distortion free energy to increase, coupled with the deformation energy stored during cold deformation, which promotes the re-dissolving of  $S'$  phase and  $\theta'$  phase. The matrix becomes re-saturated, and

provides conditions for the aggregation of solute atoms and the nucleation of re-precipitated phase. The precipitation of the re-precipitated phase occurs under rapid cold stamping strong plastic deformation. Therefore, the atomic spacing, lattice distortion and dislocation density of the alloy will change significantly, and the supersaturated matrix is in a high-energy state, resulting in re-precipitation to reduce the free energy of the matrix. The driving force is the deformation energy. Moreover, the re-precipitation of the alloy in this experiment is carried out under the conditions of low temperature, high strain and high strain rate. So, severe lattice distortion of the matrix has generated and GP zone and transition phase with coherent or semi-coherent relationship are difficult to generate. Because the interfacial relationship between the transition phase and the matrix causes the strain energy of the alloy to further increase, which results in a high free energy, the precipitation cannot be spontaneously performed. Therefore, the formation of an equilibrium phase having no coherent relationship with the matrix at the grain boundary is advantageous for reducing the free energy [22].

LIAO et al [20] calculated the formation enthalpy of  $\text{Al}_2\text{Cu}$  phase and  $\text{Al}_2\text{CuMg}$  phase according to Eq. (2). The results show that the absolute value of formation enthalpy for  $\text{Al}_2\text{CuMg}$  phase is slightly larger than that of  $\text{Al}_2\text{Cu}$  phase, which indicates that  $\text{Al}_2\text{CuMg}$  phase is easy to precipitate. However, in this experiment, since the absolute binding energy of  $\theta'$  phase is larger than that of  $S'$  phase, the alloy has a small number of fine  $\theta'$  broken particles after three passes of rapid cold stamping deformation, and the particles are not completely dissolved (Figs. 3 and 5). This provides conditions for the nucleation and growth of the  $\theta$  phase during the intermittent rapid cold stamping deformation process, thereby consuming a large number of Cu atoms in the matrix and suppressing the re-precipitation of the  $S$  phase.

#### 4.3 Effect of re-dissolution and re-precipitation of nano-precipitates on mechanical properties

It can be seen from Fig. 2 that during the multi-pass rapid cold stamping deformation process of the extruded Al–Cu–Mg alloy, the change of the hardness undergoes three stages: rapid growth in the early stage, small fluctuation in the medium term and rapid growth in the later stage. According to the comprehensive analysis in Refs. [12–15] and the results of this experimental study, the hardness change of the alloy during the rapid cold stamping process is affected by the combined effect of re-dissolution softening of precipitated phase, work hardening and re-precipitation strengthening of nano-precipitates. After two passes of rapid cold stamping

deformation, the main precipitated  $S'$  phase and  $\theta'$  phase are obviously re-dissolved (Fig. 3), which reduces the hindrance to dislocation motion and high density dislocation pile-up, weakens the effect of work hardening, and leads to a flattening of the hardness curve.

After three passes of cold stamping deformation, the  $S'$  phase is completely re-dissolved, leaving only a small number of  $\theta'$  phases (Fig. 5). The precipitation strengthening disappears and the obstacle of dislocation motion is significantly weakened. The softening of the re-dissolution is greater than the work hardening, resulting in a slight decrease in the hardness of the alloy. After four passes of rapid cold stamping deformation, the extruded alloy has a significant re-precipitation performance, and a large number of fine-grained equilibrium  $\theta$  phases are precipitated in the matrix (Fig. 6), meanwhile, the dislocation motion obstacles are enhanced, therefore the combination of precipitation strengthening and work hardening results in a significant increase in hardness.

## 5 Conclusions

(1) Rapid cold stamping deformation causes  $S'$  phase and  $\theta'$  phase to break and promote the nano-precipitate phase to dissolve. The high distortion free energy of the matrix promotes the precipitation of the equilibrium  $\theta$  phase. After four passes of rapid cold stamping deformation the hardness of the alloy increases from HB 55 to HB 125.

(2) The breaking of the brittle  $S'$  phase, the bending and breaking of the plastic  $\theta'$  phase during rapid cold stamping deformation process increase the contact area between the fractured phase and the matrix of the precipitated phase, improve the interfacial distortion energy, and promote low temperature re-dissolution of the strip-shaped  $S'$  phase and the acicular  $\theta'$  phase in the extruded alloy.

(3) Re-dissolution and re-precipitation occur in the extruded Al–Cu–Mg alloy subjected to rapid cold stamping deformation. The thick long strip-shaped  $S'$  phase and the needle-like  $\theta'$  phase in the as-extruded alloy are transformed to a fine granular  $\theta$  phase after re-dissolution and re-precipitation.

## References

- [1] WANG Zhu-tang, TIAN Rong-zhang. User manual for Al alloys and processing version [M]. 3rd ed. Changsha: Central South University Press, 2007. (in Chinese)
- [2] WILLIAMS J C, STARKE J E. Progress in structural materials for aerospace systems [J]. Acta Materialia, 2003, 51(19): 5775–5799.
- [3] LIU Man-ping, JIANG Ting-hui, XIE Xue-feng. Microstructure evolution and dislocation configurations in nanostructured Al–Mg alloys processed by high pressure torsion [J]. Transactions of

- Nonferrous Metals Society of China, 2014, 24(5): 3848–3857.
- [4] FAN Cai-he, PENG Ying-biao, YANG Hai-tang, ZHOU Wei, YAN Hong-ge. Hot deformation behavior of Al–9.0Mg–0.5Mn–0.1Ti alloy based on processing maps [J]. Transactions of Nonferrous Metals Society of China, 2017, 27(2): 289–297.
- [5] FAN Cai-he, YAN Hong-ge, PENG Ying-biao, ZHOU Wei, ZHOU Xing-ling. Microstructures and mechanical properties of spray-forming high magnesium aluminum alloy during large strain hot rolling [J]. The Chinese Journal of Nonferrous Metals, 2017, 27(1): 64–71. (in Chinese)
- [6] CHEN Xi-hong, FAN Cai-he, HU Ze-yi, YANG Jian-jun, GAO Wen-li. Research on flow stress and dynamic recrystallization behavior of Al–9Mg–1.1Li–0.5Mn alloy during hot compression process [J]. Transactions of Nonferrous Metals Society of China, 2018, 28(12): 2401–2409.
- [7] DESCHAMPS A, BASTOW T J, GEUSER F. In situ evaluation of the microstructure evolution during rapid hardening of an Al–2.5Cu–1.5Mg (wt.%) alloy [J]. Acta Materialia, 2011, 59: 2918–2927.
- [8] LAURE B, CHRISTIAN D, MATTHEW W, NIE J F. The magic thicknesses of precipitates in Sn-microalloyed Al–Cu [J]. Acta Materialia, 2012, 60: 633–644.
- [9] NOURBAKHSH S, NUTTING J. The high strain deformation of an Aluminium–4% copper alloy in the supersaturated and aged conditions [J]. Acta Metallurgica, 1980, 28(3): 357–365.
- [10] SENKOV O N, FROES F H, STOLYAROV V V. Microstructure and microhardness of an Al–Fe alloy subjected to severe plastic deformation and aging [J]. Nanostruct Mater, 1998, 25(10): 691–698.
- [11] MURAYAMA M, HORITA Z, HONO K. Microstructure of two-phase Al–1.7at%Cu alloy deformed by equal-channel angular pressing [J]. Acta Mater, 2001, 49(1): 21–29.
- [12] ZHANG Zi-zhao, XU Xiao-chang, HU Nan, QU Xiao, CHEN Zhen-xiang. Re-ageing behavior of Al–Cu alloy after re-dissolution of precipitated phases caused by severe plastic deformation [J]. Journal of Central South University (Science and Technology), 2010, 41(5): 1782–1790. (in Chinese)
- [13] ZHANG Zi-zhao, XU Xiao-chang, LIU Zhi-yi, XIA Qing-kun, ZENG Su-min. Re-precipitate behavior of supersaturated solid solution of Al–Cu alloy caused by severe plastic deformation during subsequent deformation [J]. The Chinese Journal of Nonferrous Metals, 2009, 19(11): 1962–1968. (in Chinese)
- [14] XU Xiao-chang, LIU Zhi-yi, LI Yun-tao. Evolution of precipitates of Al–Cu alloy during equal-channel angular pressing at room temperature [J]. Transactions of Nonferrous Metals Society of China, 2008, 18(5): 1047–1052.
- [15] DANG Peng, XU Xiao-chang, LUI Zhi-yi, YU Wen-bin, NING Ai-lin, ZENG Su-min. Investigation on dissolution of precipitates in Al alloy deformed by equal-channel angular pressing and multi-axial compression [J]. Transactions of Materials and Heat Treatment, 2007, 28(50): 82–85.
- [16] STYLES M J, MARCEAU R K W, BASTOW T J, BRAND H E A, GIBSON M A, HUTCHINSON C R. The competition between metastable and equilibrium  $S(\text{Al}_2\text{CuMg})$  phase during the decomposition of Al–Cu–Mg alloys [J]. Acta Materialia, 2015, 98(1): 64–80.
- [17] VASILS L S, LONMAEV I L, ELSUKOV E P. On the analysis of the mechanisms of the strain-induced dissolution of phases in metals [J]. Physics of Metals and Metallography, 2006, 102(2): 186–197.
- [18] PUGH S F. Relations between the elastic moduli and the plastic properties of polycrystalline pure metals [J]. The London, Edinburgh, and Dublin Philosophical Magazine and Journal of Science, 1954, 45(367): 823–843.
- [19] ZHANG J, HUANG Y N, MAO C. Structural, elastic and electronic properties of  $\theta(\text{Al}_2\text{Cu})$  and  $S(\text{Al}_2\text{CuMg})$  strengthening precipitates in Al–Cu–Mg series alloys: First-principles calculations [J]. Solid State Communications, 2012, 152(23): 2100–2104.
- [20] LIAO Fei, FAN Shi-tong, DENG Yun-lai, ZHANG Jin. First-principle calculations of mechanical properties of  $\text{Al}_2\text{Cu}$ ,  $\text{Al}_2\text{CuMg}$  and  $\text{MgZn}_2$  intermetallics in high strength aluminum alloys [J]. Journal of Aeronautical Materials, 2016, 36(6): 1–8. (in Chinese)
- [21] YU Yong-ling. Principles of metallography [M]. 2nd ed. Beijing: Metallurgical Industry Press, 2013. (in Chinese)
- [22] STRAUMAL B B, BARETZKY B, MAZILKIN A A. Formation of nanograined structure and decomposition of supersaturated solid solution during high pressure torsion of Al–Zn and Al–Mg alloys [J]. Acta Materialia, 2004, 52: 4469–4478.

## 快速冷冲 Al–Cu–Mg 合金纳米析出相的回溶及再析出行为

范才河<sup>1</sup>, 欧玲<sup>1</sup>, 胡泽艺<sup>1</sup>, 阳建君<sup>1</sup>, 陈喜红<sup>2</sup>

1. 湖南工业大学 冶金与材料工程学院, 株洲 412007;
2. 中国中车株洲电力机车有限公司, 株洲 412007

**摘要:** 采用高分辨透射电镜(TEM)、X射线衍射(XRD)、能谱分析(EDS)和硬度测试等手段, 研究快速冷冲强变形过程中喷射成形细晶 Al–Cu–Mg 合金纳米析出相的回溶及再析出行为。实验结果表明: 挤压态 Al–Cu–Mg 合金在快速冷冲强变形过程中发生明显的回溶和再析出现象, 塑性  $\theta$  相的回溶速度小于脆性  $S'$  相的回溶速度。经 3 道次快速冷冲强变形后挤压态合金中的长片状  $S'$  相和针状  $\theta$  相基本回溶, 形成过饱和固溶体, 合金经 4 道次快速冷冲变形后析出大量细小的颗粒状平衡相  $\theta$  相。快速冷冲强变形导致  $S'$  相和  $\theta$  相发生破断, 促使纳米析出相回溶。基体的高畸变自由能加速平衡  $\theta$  相的析出, 且合金硬度在快速冷冲过程中显著增大, 由 HB 55 增加到 HB 125。

**关键词:** Al–Cu–Mg 合金; 快速冷冲; 纳米析出相; 回溶; 再析出

(Edited by Wei-ping CHEN)